Sand Maria (Orcid ID: 0000-0003-0256-7468)
Samset Bjørn, Hallvard (Orcid ID: 0000-0001-8013-1833)
Tsigaridis Kostas (Orcid ID: 0000-0001-5328-819X)
Bauer Susanne, E. (Orcid ID: 0000-0001-7823-8690)
Myhre Gunnar (Orcid ID: 0000-0002-4309-476X)

Black Carbon and Precipitation: an Energetics Perspective

M. Sand[1], B. H. Samset[1], K. Tsigaridis[2,3], S. E. Bauer[3,2], and G. Myhre[1]

[1]CICERO Center for International Climate Research – Oslo, 0318 Oslo, Norway

[2]Center for Climate Systems Research, Columbia University, New York, NY 10025, USA

[3]NASA Goddard Institute for Space Studies, New York, NY 10025, USA

Corresponding author: Maria Sand (maria.sand@cicero.oslo.no)

Key Points:

- The strong atmospheric shortwave absorption by black carbon suppresses precipitation.
- Rapid adjustments decrease the direct radiative effect of black carbon in two independent models
- Even though the underlying processes are strikingly similar in the models, the resulting change in precipitation and temperature by black carbon differ

This article has been accepted for publication and undergone full peer review but has not been through the copyediting, typesetting, pagination and proofreading process which may lead to differences between this version and the Version of Record. Please cite this article as doi: 10.1029/2019JD032239

Abstract

Black carbon aerosols (BC) influence precipitation through a range of processes. The climate response to the presence of BC is however highly dependent on its vertical distribution. Here, we analyze the changes in the energy budget and precipitation impacts of adding a layer of BC at a range of altitudes in two independent global climate models. The models are run with atmosphere-only and slab ocean model setup to analyze both fast and slow responses, respectively. Globally, precipitation changes are tightly coupled to the energy budget. We decompose the precipitation change into contributions from absorption of solar radiation, atmospheric longwave radiative cooling, and sensible heat flux at the surface. We find that for atmosphere-only simulations, BC rapidly suppress precipitation, independent of altitude, mainly because of strong atmospheric absorption. This reduction is offset by increased atmospheric radiative longwave cooling and reduced sensible heat flux at the surface, but not of sufficient magnitude to prevent reduced precipitation. On longer timescales, when the surface temperature is allowed to respond, we find that the precipitation increase associated with surface warming can compensate for the initial reduction, particularly for BC in the lower atmosphere. Even though the underlying processes are strikingly similar in the two models, the resulting change in precipitation and temperature by BC differ quite substantially.

Plain Language Summary

Soot particles change precipitation by absorbing solar radiation and heating the surrounding air. The atmosphere rapidly adjusts to this added warming by changing relative humidity, clouds and precipitation. We use two climate models to investigate these rapid adjustments in the atmosphere caused by soot particles. We insert soot particles in different vertical layers in the models and find that soot particles quickly warm the atmosphere and reduce precipitation. Soot particles at higher altitudes, stabilize the atmosphere and increase cloud cover located below. Given all the processes soot particles influence in the atmosphere, the similarities in underlying processes by the two climate models are striking. The resulting change in precipitation and temperature differ quite substantially.

1 Introduction

Black carbon (BC) aerosols can influence precipitation by absorbing solar radiation and changing the atmospheric heating rates (Ming et al., 2010; Ramanathan et al., 2001). The atmosphere rapidly adjusts to this added heat by changing the clouds, relative humidity and precipitation. These effects, which occur independently of any subsequent change in surface temperature, are commonly termed rapid adjustments to the instantaneous (direct) radiative forcing of BC (Boucher et al., 2013). Different climate forcers, such as BC, scattering aerosols or CO_2, can induce very different rapid adjustments (on short timescale typically days) (Smith et al., 2018; Stjern et al., 2017). Slow feedbacks on the other hand, caused by the response in surface temperatures, seems to be less dependent on the initial climate forcer (Richardson et al., 2018). The separation between rapid adjustments and the feedback from surface temperature change, often termed the fast response and slow response respectively, has proven to be useful when studying precipitation (Andrews et al., 2010; Samset et al., 2016). The fast response can further be divided into the instantaneous (or initial) perturbation and the rapid adjustment (Sherwood et al., 2015). The modeled precipitation response to BC perturbations is far more diverse than for other climate drivers (Samset et al., 2016). This is partly because of the complexity of BC RF on the climate, the vertical dependence on the climate response of BC, and the large negative fast precipitation changes due to strong absorption of solar radiation, all of which may be treated differently between current climate models.

Both the magnitude and sign of changes in surface temperatures depend on the vertical distribution of BC. BC at low altitudes can warm the surface (and the surrounding air), while BC at high altitudes have a weak positive or negative surface temperature change, by absorbing and reducing downwelling solar radiation (Ramanathan & Carmichael, 2008). This is especially true in the Arctic, where the strong static stability limits vertical mixing of air masses (Flanner, 2013; Sand et al., 2013). The net impact of BC on clouds is complex (Koch & Del Genio, 2010). Depending on the altitude, BC can either reduce or increase the cloud cover (Ban-Weiss et al., 2012; Hansen et al., 2005). For instance, by warming the surrounding air, BC can evaporate nearby clouds or inhibit cloud formation (Ackerman et al., 2000; Hansen et al., 1997). BC located above clouds on the other hand, may increase the static stability in the atmosphere and increase stratocumulus clouds below (Johnson et al., 2004). BC located below clouds can promote convection and thereby increase cloud cover (Feingold et al., 2005). Therefore, the estimate of the rapid adjustment (previously often referred to as semi-direct effect) will be highly dependent of both the simulated cloud and BC fields in each model (Hodnebrog et al., 2014). Despite the numerous ways BC can impact clouds, however, cloud responses from BC at different locations relative to clouds are broadly similar in GCMs and large eddy simulations (LES) (Koch & Del Genio, 2010). There are observational evidences of rapid adjustments in polluted, smoky conditions that cause a reduction in low clouds (Ackerman et al., 2000; Koren et al., 2004; Koren et al., 2005; Li et al., 2011). Whether this reduction is due to increased stabilization that suppresses cloud formation or a 'burn-off effect' of BC absorption in cloud droplets is difficult to distinguish.

Previously, Samset and Myhre (2015) inserted BC in different model layers in the Community Atmosphere Model version 4 (CAM4) to investigate the climate response to BC at a given altitude. They found that the positive instantaneous RF by BC is strongly offset by negative rapid adjustments in the atmosphere. Furthermore, both the instantaneous radiative aerosol effect and the rapid adjustment of BC strengthens with altitude of about the same magnitude, so the net effective radiative forcing is nearly constant with altitude of BC. The precipitation response on a long timescale was found to be negative at all altitudes, except when BC was inserted between the surface and 900 hPa. Analysis from the Precipitation Driver Response Model Intercomparison Project (PDRMIP) suggests that the rapid adjustments of BC are negative and offset more than half of its instantaneous effect (Smith et al. 2018).

Here we analyze the precipitation response to BC inserted at different altitudes in more detail, by adding one more model to the analysis (GISS ModelE) and by separating between the rapid adjustments in the atmosphere and the slow feedbacks linked to surface temperature changes. To understand the precipitation changes due to BC we analyze the energy budget. Precipitation changes are constrained by the global energy budget, and there is a balance between the latent heat of condensation released by precipitation and the net atmospheric cooling. We therefore decompose the precipitation response into contributions from absorption of solar radiation, atmospheric longwave radiative cooling, and sensible heat flux at the surface.

2 Methods

2.1 Climate models

We use two global climate models; The National Center for Atmospheric Research (NCAR) Community Atmosphere Model version 4 (CAM4) (Neale et al., 2010), and the Goddard Institute for Space Studies (GISS) ModelE NonINTeractive ('NINT') version 2.1 (GISS-E2) (Schmidt et al., 2014). CAM4 is run with a horizontal resolution of 1.9°×2.5° and a vertical

resolution of 26 layers. The top layer is at 3hPa (approx. 40 km height). GISS-E2 is run with a horizontal resolution of 2°×2.5° and a vertical resolution of 40 layers where the top model layer is at 0.1 hPa (approx. 60 km height). The aerosol fields in both models are prescribed, there are no aging processes included, and BC is assumed fully externally mixed. This is a crude assumption for BC, but here we study the response to an amount of absorption rather than a realistic absorption enhancement (Fierce et al. 2020). Aerosol-cloud microphysical interactions are not included i.e. the only feedback from BC aerosols on cloud formation and properties comes through local heating and impacts on lapse rates, humidity, and circulation.

2.2 Experimental setup

We add a globally uniform burden of 3.0 mg m^{-2} BC in each model layer; 26 layers in CAM4 and 30 layers (the lowest of total 40) in GISS-E2; and perform separate simulations for each addition. Note that since the vertical layers in the two models differ, the thickness and thus the BC mass mixing ratio vary. To separate the fast response to the addition of BC from the surface temperature response BC, we run the models with fixed sea surface temperatures (fSST) for each perturbed simulation (26 simulations for CAM4 and 30 for GISS-E2) and compare each simulation with an unperturbed baseline simulation (year 2000). We analyze the average of the last 5 years of each simulation of a total of 7 years for CAM4 and the last 10 years of total 15 years for GISS-E2. The reason for the different simulation years, is because simulations with CAM4 was already performed in the previous study (Samset and Myhre, 2015). To investigate the total response of BC, i.e. including surface temperature change, we run each model 30 years with a slab ocean model (SOM) where the temperature of the ocean is calculated based on the mixed-layer depth and the surface energy fluxes. Here we analyze the average of the last 10 years for both models. For CAM4, not all layers where perturbed in the SOM setup to save computational time.

2.3 Energy budget

The instantaneous radiative forcing (IRF) and the rapid adjustments is estimated as described below following Chung and Soden (2015).

$$IRF = ERF - RA \quad (1)$$

ERF is the effective radiative forcing and RA are rapid adjustments, where ERF is the top of the atmosphere radiation imbalance from fSST simulations. The IRF is calculated as a second call in the radiation code (with and) without any scattering/absorption of aerosols, and the RA is calculated as a residual.

Inspired by O'Gorman et al. (2012), we analyze the energy budget to understand how BC influence precipitation. On a global scale the latent heat released by precipitation will be balanced by the net atmospheric cooling:

$$L_c \Delta P = \Delta Q + \Delta H = \Delta LWC - \Delta SWA - \Delta SH + \Delta H \quad (2)$$

L_c is the latent heat of condensation, P is precipitation, Q is the net atmospheric cooling, LWC is the atmospheric longwave cooling, SWA is the atmospheric SW absorption and SH is the sensible heat flux. When we separate the precipitation response between ocean and land, we also include the dry static energy flux divergence H (Muller & O'Gorman, 2011; Richardson et al., 2016). H is calculated as a residual. LWC is purely a rapid adjustment through changes in temperature, water vapor or clouds since no LW absorption of BC is included in the two GCMs, whereas the SWA is mainly due to instantaneous perturbation of BC but also a result of the rapid adjustments.

3 Results

3.1 Radiative forcing of BC per altitude

In Figure 1 we show how BC at different altitudes alter the radiative fluxes at the TOA and thus atmospheric energy budget. Fig 1 a) shows the instantaneous radiative forcing (IRF), the effective radiative forcing (ERF) and the rapid adjustments at TOA, for BC added at the altitude given on the y-axis. The ERF, i.e. the net energy imbalance at TOA (SW+LW) is positive for all altitudes (solid line). In CAM4, the net flux is strongest for BC added close to the surface. The IRF is positive and strengthens with altitude of BC (dotted line). IRF increases with height because i) the underlying albedo is higher for BC located above clouds, ii) more Rayleigh scattering (and hence more BC absorption), and iii) less competition from other absorbing components like water vapor and ozone higher up in the atmosphere (Samset & Myhre, 2011; Zarzycki & Bond, 2010). The IRF is larger than ERF at TOA for all BC heights except for BC added close to the surface in CAM4. The dash-dotted curve shows the rapid adjustments and this curve is the difference between the IRF and ERF. The RAs are negative and offset the BC IRF for all layers except for BC close to the surface. In both models the ERF is fairly constant with altitude of BC with largest deviations below 900 hPa and above 200 hPa. The IRF is somewhat stronger in magnitude in GISS-E2 relative to CAM4, especially at high altitudes. On the other hand, the RA is slightly weaker in magnitude in GISS-E2 compared to CAM4. Since the ERF is the sum of IRF and rapid adjustment, the difference between GISS-E2 and CAM4 is larger than the individual components of IRF and rapid adjustments. We will discuss the rapid adjustments and clouds in more detail in 3.3.

The changes in the TOA radiative fluxes contribute to changes in the atmospheric energy budget as illustrated in 1b). The SW absorption is strong and positive and increases with height. The SW absorption by BC is larger for GISS-E2 (red lines) compared to CAM4 (blue), similar to the IRF at the TOA. This is because the total surface temperature response per BC height (shown in Fig S1 in supplement) is larger for GISS-E2 compared to CAM4. Also, the atmospheric temperature change in the layer BC is inserted is larger for GISS-E2 compared to CAM4 above 950 hPa (Fig S1). The BC induced increase in SW absorption and atmospheric temperatures cause more radiation to be emitted to space (and downwards), increasing radiative LW cooling. The LW cooling increase for all layers but is smaller than the SW absorption. The sensible heat flux is negative for all layers. This means that heat is transferred from the atmosphere to the surface for all layers BC is added. The decrease in sensible heat flux is larger for BC added near the surface.

Figure 1c) shows the surface temperature response in the SOM simulations normalized to the TOA ERF per layer. i.e. the climate sensitivity parameter. The climate sensitivity parameter is positive for BC added in the lowest layers and decrease in magnitude the higher in the atmosphere BC is added. The normalized surface temperature response is similar in the two models, except for the spike in GISS-E2 at 900 hPa, which is linked to the (global mean) ERF being close to zero (Fig 1a). For BC added in 900 hPa in GISS-E2, the ERF is positive over land, but negative over tropical oceans (not shown). The climate sensitivity parameter shows a similar shape as to Hansen et al. (1997) Fig 8a., where a ghost forcing of 4 W/m^2 was introduced at arbitrary heights.

The normalized precipitation response for both atmosphere-only (fSST) and SOM simulations is shown in Fig1d. Here, the dotted lines represent the rapid adjustments from the atmosphere-only simulations. The solid lines represent the total response (in which also the

surface temperature is also allowed to influence precipitation). Both the fast and total precipitation response is negative for all heights, except for the total response near the surface, where the precipitation increases. The precipitation decrease per forcing is larger for CAM4 compared to GISS-E2. As in Fig 1c, the spikes are caused by a near-zero ERF for BC added at these levels.

To sum up; BC strongly absorbs solar radiation, which leads to a warming of the atmosphere and more radiation emitted to space. The direct radiative effect caused by the absorption of BC is positive and becomes stringer with altitude. However, the net radiative imbalance at TOA, the ERF, is smaller, because rapid adjustments are generally negative and offset the direct effect of BC. The SW absorption of BC leads to a reduction in precipitation, except for BC near the surface on long timescales. We will look at this in more detail in Fig2 and Fig 3.

3.2 The Energetic Perspective of BC on precipitation

In Figure 2 we decompose the fast precipitation response into the energy budget terms from Equation 2 and split between global, land and ocean mean, respectively. Furthermore, Equation 2 shows the budget is balanced, and the sign convention for SW absorption and sensible heat flux is negative. Inserting BC results in a decrease in precipitation at all altitudes studied here, in both models, as illustrated by the blue dots. Globally, the precipitation decrease is strongest for BC added around 200 hPa. The negative precipitation response is mostly due to an increase in atmospheric SW absorption (yellow bars). The precipitation reduction is partly offset by an increase in LW atmospheric cooling (light blue bars) and a reduction in sensible heat flux (green bars) as the atmosphere warms and more radiation is emitted to space and downwards. For BC located above 200 hPa, the LW cooling increases and almost balances the SW absorption.

The precipitation reductions are stronger over the oceans compared to land, mainly due to a positive dry static energy flux and a larger reduction in sensible heat flux over land. When the dry static energy flux is positive over land (and negative over oceans), it means energy is transported from the land to the oceans. The positive dry static energy flux over land implies that circulation changes over land dampens the reduction in precipitation.

We note that in both models, the global energy budget is closed, i.e. the LdP term calculated from the modeled precipitation change itself is identical to the one calculated using the energy balance terms in Equation 2.

Figure 3 shows the total response from the slab ocean simulations. Here we see that on longer timescales BC may increase precipitation by warming the surface. For BC added near the surface, a positive surface temperature response and an increase in water vapor increases the longwave radiative cooling. This leads to an increase in precipitation. In general, the longwave radiative cooling from an increase in temperature at the surface and in the atmosphere is larger in the slab ocean simulations compared to the fSST simulations, making the precipitation change less negative on longer timescales.

3.3 Rapid adjustments

In Figure 1 a) we showed that the global mean rapid adjustments of BC were negative, except close to the surface. The BC rapid adjustments vary regionally. This can be seen in Figure 4, where the geographical distribution of the rapid adjustments from Figure 1 a) is plotted for five selected BC levels (given in hPa on top left of each panel). For BC injected at the surface

layer, the global mean rapid adjustments are positive, with high values in the Arctic and over the oceans. The areas with positive values are co-located with the largest reductions in low clouds (Figure 5 a) and surface warming (Fig S2). The global mean rapid adjustments become increasingly negative with BC height.

The low-level cloud threshold in the two models is bounded by the surface to up to 680-700hPa, which means that in the two lowest panels in Fig 5 a) BC is added within the low cloud layer. Here we see that the global mean low cloud cover decrease, especially for marine stratocumulus clouds near coastal areas. Global mean low cloud cover increases when BC is added at higher altitudes. This is consistent with a stabilization of the atmosphere, and less convective activity. At these BC insertion altitudes, the models differ in areas with marine stratocumulus clouds near coastal areas, where the low clouds decrease in GISS-E2 and increase in CAM4.

The rapid adjustments are positive in areas with the largest increase in high clouds (Figure 5 b), in particular for CAM4. The two top panels lie within the high-level cloud threshold above 400hPa. High clouds increase globally by 30-50% in CAM4 for BC added to these top layers (above 350 hPa). For GISS-E2 the pattern is quite different, with a reduction in high clouds. The exception is subtropical oceanic areas near South Africa and South America, where also CAM4 shows the largest increases in high clouds. These results are consistent with Fig 6, where the overall changes are similar between the two models with different magnitude of cloud changes. To summarize; BC located near the surface reduces low cloud cover, while BC added at higher altitudes enhances low clouds. While the low cloud response is fairly similar between the models, this is not the case for high clouds. At high altitudes BC increases the high cloud cover in CAM4 but reduces the high cloud cover in GISS-E2 except in a thin belt south of the ITZC, where also CAM4 shows maximum increase in high clouds. This difference is mainly due to enhanced warming at higher altitudes in GISS-E2 compared to CAM4 as we will show next.

Changes in the vertical profiles of global mean temperature, relative humidity, and cloud fraction in shown in Figure 6, for 7 selected BC insertions (given as colored dots on the y-axis). The warming of the atmosphere by BC is largest in the layer BC is inserted and increase with injection height layer (Figure 5 a), since the local heating rates depends on the density. The warming spreads to layers above and below this layer, with strong similarities between CAM4 and GISS-E2. This vertical energy transport is sufficiently strong that BC added to layer in the upper troposphere leads to warming in the lower stratosphere. Temperature and relative humidity are inversely related, where the increased temperature induced water vapor is not strong enough to compensate the temperature itself. Relative humidity decreases in the air surrounding BC, but increases above and below the added BC layer, especially for BC added at high altitudes. BC also reduces the fraction of surrounding clouds, but increases the amount of clouds located below, largely following the pattern of relative humidity. For BC added at 600 hPa and higher, cloud cover also increases above the added BC layer, especially in CAM4.The enhanced warming in the layer BC is inserted just below 200hPa in GISS-E2 compared to CAM4 (dark blue lines) partly explain why the high cloud fraction is decreasing here for GISS-E2. For BC added in the lower and middle troposphere the changes in relative humidity and clouds are similar between the two models. For BC added in the upper troposphere on the other hand, the differences in relative humidity

and corresponding changes in high clouds are larger. To fully understand these differences, targeted simulations and additional analysis are needed.

Even though the high cloud response differs between the models, the rapid adjustments are quite similar between the models. This is due to compensating effects. Figure 7 shows the geographical distribution of LW cooling and SW absorption for the same five selected BC layers as in Fig 4 and Fig 5. We find a large decrease in the LW cooling linked to an increase in high clouds for BC added at high altitudes for both models, counteracting the general LW induced cooling. This partly explains why the rapid adjustments are so similar between the two models despite the relatively large differences in the high cloud response. The SW absorption increases with BC height with a broader homogeneous geographical pattern. The stronger SWA over land is due to higher surface albedo. SWA is stronger at high altitude BC in regions with high abundance of clouds.

Figure 8 shows the geographical distribution of sensible heat flux change for five selected BC layers. Sensible heat is here given as a reduction in the upward flux. The added warming reduces sensible heat flux from the ground to the atmosphere, both over land and oceans (note that these are the fixed SST runs), but with an inhomogeneous geographical pattern. Interestingly, the sensible heat flux is also reduced when BC is added at higher altitudes. The pattern of sensible heat flux changes is overall very similar between the two models.

Figure 9 shows the zonal mean temperature response for BC added in four different altitudes. This is the total response (slow + fast) calculated from the SOM simulations. BC heats the layer in which it is inserted, and this warming spreads to layers above and below. The warming is larger for higher latitudes. For CAM4 the warming from BC added in the surface layer goes up to above 400 hPa at higher latitudes. When BC is added at high altitudes, the absorbed energy is efficiently transported to higher levels in the tropics.

4 Discussion and conclusions

When BC is abruptly added to the atmosphere, as we have done here through a set of idealized simulations in two independent climate models, the increased absorption of solar radiation leads to a range of rapid adjustments; altered stability, cloud fractions, relative humidity and precipitation. We have shown that these rapid adjustments are negative in terms of forcing at TOA at all layers, except for BC added in the two lowest model layers, and offset the positive IRF due to BC. BC quickly warms the model layer where it is inserted, reducing the relative humidity and the cloud fraction. The warming is then transported both upwards and downwards in the models. This stabilizes the atmosphere and further increases the cloud cover below, whereas it often causes larger instability and increasing the clouds above BC added to the middle and upper troposphere. BC rapidly reduces precipitation in all layers by strongly absorbing solar radiation. The added heat also reduces the sensible heat flux at the surface and increase the radiative longwave cooling. Both these mechanisms contribute to precipitation increase, but the short-wave absorption offsets this increase. The precipitation decrease is mainly occurring over the oceans.

Our estimates of the atmospheric rapid adjustments are dependent on the BC-cloud interactions and the amount of BC absorption, both which are sensitive to the representation of BC (and clouds) in the models (Bauer et al., 2010).

A key result from this study is the striking similarity on the underlying processes in the two models. The vertical profile of atmospheric temperatures, clouds and relative humidity's changes from BC have similar pattern between the two, with some smaller geographical and magnitude differences. This leads to similar TOA rapid adjustments in the two models and they have almost the same shape of the IRF. Furthermore, BC leads to highly comparable change in SW absorption, LW cooling and sensible heat flux for the two models.

In this idealized study, we have added globally uniform levels of BC. In reality, BC is mainly emitted in areas with large industrial activity and/or biomass burning. The total rapid adjustments of BC will depend on emission location and lifetime. Recent studies suggest that BC has a lower lifetime (e.g. Bauer et al. 2013; Hodnebrog et al. 2014, Schwarz et al. 2010). A lower lifetime will impact atmospheric BC profiles, emphasising more low-level BC. The ERF depends on the vertical profile of BC. As apparent in Fig 1b, the higher BC is in the atmosphere, the stronger direct aerosol effect and rapid adjustments, as also shown in other studies (e.g. Vuolo et al 2014, Samset et al. 2013). To quantify the total impact on climate by BC we need better estimates of BC mass absorption coefficients (Fierce et al. 2020) and BC lifetime.

Acknowledgments

M.S. was founded by the Research Council of Norway (RCN), through the grants BlackArc (240921) and AC/BC (240372). BHS and GM also acknowledge funding from RCN, through AC/BC (240372) and NetBC (244141). GISS ModelE is supported by the NASA Modeling, Analysis, and Prediction program, and computer resources were provided by the NASA High-End Computing (HEC). The CESM project is supported by the National Science Foundation and the Office of Science (BER) of the U.S. Department of Energy.

The model data from GISS ModelE and CAM4 supporting the findings of this study is openly available at NIRD Research Data Archive doi:10.11582/2020.00026 .

References

Ackerman, A. S., Toon, O. B., Stevens, D. E., Heymsfield, A. J., Ramanathan, V., & Welton, E. J. (2000). Reduction of Tropical Cloudiness by Soot. *Science, 288*(5468), 1042-1047. doi:10.1126/science.288.5468.1042

Andrews, T., Forster, P. M., Boucher, O., Bellouin, N., & Jones, A. (2010). Precipitation, radiative forcing and global temperature change. *Geophysical Research Letters, 37*.

Ban-Weiss, G., Cao, L., Bala, G., & Caldeira, K. (2012). Dependence of climate forcing and response on the altitude of black carbon aerosols. *Climate Dynamics, 38*(5-6), 897-911. doi:10.1007/s00382-011-1052-y

Bauer, S., Menon, S., Koch, D., Bond, T., & Tsigaridis, K. (2010). A global modeling study on carbonaceous aerosol microphysical characteristics and radiative effects. *Atmos. Chem. Phys, 10*, 7439-7456.

Boucher, O., D. Randall, P. Artaxo, C. Bretherton, G. Feingold, P. Forster, V.-M. Kerminen, Y. Kondo, H. Liao, U. Lohmann, P. Rasch, S.K. Satheesh, S. Sherwood, B. Stevens and X.Y. Zhang. (2013). Clouds and Aerosols. In: Climate Change 2013: The Physical Science Basis. Contribution of Working Group I to the Fifth Assessment Report of the Intergovernmental Panel on Climate Change [Stocker, T.F., D. Qin, G.-K. Plattner, M. Tignor, S.K. Allen, J. Boschung, A. Nauels, Y. Xia, V. Bex and P.M. Midgley (eds.)]. Cambridge University Press, Cambridge, United Kingdom and New York, NY, USA.

Chung, E.-S., & Soden, B. J. (2015). An assessment of methods for computing radiative forcing in climate models. *Environmental Research Letters, 10*(7), 074004. doi:10.1088/1748-9326/10/7/074004

Feingold, G., Jiang, H., & Harrington, J. Y. (2005). On smoke suppression of clouds in Amazonia. *Geophysical Research Letters, 32*(2). doi:doi:10.1029/2004GL021369

Fierce, L., Onasch, T. B., Cappa, C. D., Mazzoleni, C., China, S., Bhandari, J., Davidovits, P., Fischer, D. A., Helgestad, T., Lambe, A. T., Sedlacek, A. J., Smith, G. D., & Wolff, L. (2020). Radiative absorption enhancements by black carbon controlled by particle-to-particle heterogeneity in composition. *Proceedings of the National Academy of Sciences*, 201919723. doi:10.1073/pnas.1919723117

Flanner, M. G. (2013). Arctic climate sensitivity to local black carbon. *Journal of Geophysical Research: Atmospheres, 118*, 1-12. doi:10.1002/jgrd.50176

Hansen, J., Sato, M., & Ruedy, R. (1997). Radiative forcing and climate response. *J. Geophys. Res, 102*(D6), 6831–6864.

Hansen, J., Sato, M., Ruedy, R., Nazarenko, L., Lacis, A., Schmidt, G. A., Russell, G., Aleinov, I., Bauer, M., Bauer, S., Bell, N., Cairns, B., Canuto, V., Chandler, M., Cheng, Y., Del Genio, A., Faluvegi, G., Fleming, E., Friend, A., Hall, T., Jackman, C., Kelley, M., Kiang, N., Koch, D., Lean, J., Lerner, J., Lo, K., Menon, S., Miller, R., Minnis, P., Novakov, T., Oinas, V., Perlwitz, J., Perlwitz, J., Rind, D., Romanou, A., Shindell, D., Stone, P., Sun, S., Tausnev, N., Thresher, D., Wielicki, B., Wong, T., Yao, M., & Zhang, S. (2005). Efficacy of climate forcings. *Journal of Geophysical Research: Atmospheres, 110*, D18104. doi:10.1029/2005JD005776

Hodnebrog, Ø., Myhre, G., & Samset, B. H. (2014). How shorter black carbon lifetime alters its climate effect. *Nature Communications, 5*, 5065. doi:10.1038/ncomms6065

Johnson, B. T., Shine, K. P., & Forster, P. M. (2004). The semi-direct aerosol effect: Impact of absorbing aerosols on marine stratocumulus. *Quarterly Journal of the Royal Meteorological Society, 130*(599), 1407-1422. doi:10.1256/qj.03.61

Koch, D., & Del Genio, A. D. (2010). Black carbon semi-direct effects on cloud cover: review and synthesis. *Atmos. Chem. Phys., 10*(16), 7685-7696. doi:10.5194/acp-10-7685-2010

Koren, I., Kaufman, Y. J., Remer, L. A., & Martins, J. S. (2004). Measurements of the effect of Amazon smoke on inhibitation of cloud formation. *Science*, 303, 1342–1345. doi:10.1126/science.1089424

Koren, I., Kaufman, Y. J., Rosenfeld, D., Remer, L., & Rudich, Y. (2005). Aerosol invigoration and restructuring of Atlantic convective clouds. *Geophysical Research Letters*, 32. doi:10.1029/2005GL023187

Li, Z., Niu, F., Fan, J., Liu, Y., Rosenfeld, D., & Ding, Y. (2011). Long-term impacts of aerosols on the vertical development of clouds and precipitation. *Nature Geoscience*, 4(12), 888–894. doi:10.1038/ngeo1313

Ming, Y., Ramaswamy, V., & Persad, G. (2010). Two opposing effects of absorbing aerosols on global-mean precipitation. *Geophysical Research Letters, 37*(13), L13701. doi:10.1029/2010GL042895

Muller, C. J., & O'Gorman, P. A. (2011). An energetic perspective on the regional response of precipitation to climate change. *Nature Climate Change, 1*(5), 266-271. doi:10.1038/nclimate1169

Neale, R. B., Richter, J. H., Conley, A. J., Park, S., Lauritzen, P. H., Gettelman, A., Williamson, D. L., Rasch, P. J., Vavrus, S. J., Taylor, M. A., Collins, W. D., Zhang, M., & Lin, S.-j. (2010). *Description of the NCAR Community Atmosphere Model (CAM 4.0)*.

O'Gorman, P. A., Allan, R. P., Byrne, M. P., & Previdi, M. (2012). Energetic Constraints on Precipitation Under Climate Change. *Surveys in Geophysics, 33*(3), 585-608. doi:10.1007/s10712-011-9159-6

Ramanathan, V., & Carmichael, G. (2008). Global and regional climate changes due to black carbon. *Nature Geoscience, 1*(4), 221.

Ramanathan, V., Crutzen, P. J., Kiehl, J. T., & Rosenfeld, D. (2001). Aerosols, Climate, and the Hydrological Cycle. *Science, 294*(5549), 2119-2124. doi:10.1126/science.1064034

Richardson, T. B., Forster, P. M., Andrews, T., Boucher, O., Faluvegi, G., Fläschner, D., Hodnebrog, Ø., Kasoar, M., Kirkevåg, A., Lamarque, J.-F., Myhre, G., Olivié, D., Samset, B. H., Shawki, D., Shindell, D., Takemura, T., & Voulgarakis, A. (2018). Drivers of Precipitation Change: An Energetic Understanding. *Journal of Climate, 31*(23), 9641-9657. doi:10.1175/jcli-d-17-0240.1

Richardson, T. B., Forster, P. M., Andrews, T., & Parker, D. J. (2016). Understanding the Rapid Precipitation Response to CO2 and Aerosol Forcing on a Regional Scale. *Journal of Climate, 29*(2), 583-594. doi:10.1175/jcli-d-15-0174.1

Samset, B. H., & Myhre, G. (2011). Vertical dependence of black carbon, sulphate and biomass burning aerosol radiative forcing. *Geophysical Research Letters, 38*(24), L24802. doi:10.1029/2011GL049697

Samset, B. H., & Myhre, G. (2015). Climate response to externally mixed black carbon as a function of altitude. *Journal of Geophysical Research: Atmospheres, 120*(7), 2913-2927. doi:10.1002/2014JD022849

Samset, B. H., Myhre, G., Forster, P. M., Hodnebrog, Ø., Andrews, T., Faluvegi, G., Fläschner, D., Kasoar, M., Kharin, V., Kirkevåg, A., Lamarque, J. F., Olivié, D., Richardson, T., Shindell, D., Shine, K. P., Takemura, T., & Voulgarakis, A. (2016). Fast and slow precipitation responses to individual climate forcers: A PDRMIP multimodel study. *Geophysical Research Letters, 43*(6), 2782-2791. doi:10.1002/2016GL068064

Sand, M., Berntsen, T. K., Kay, J. E., Lamarque, J. F., Seland, Ø., & Kirkevåg, A. (2013). The Arctic response to remote and local forcing of black carbon. *Atmos. Chem. Phys., 13*(1), 211-224. doi:10.5194/acp-13-211-2013

Schmidt, G. A., Kelley, M., Nazarenko, L., Ruedy, R., Russell, G. L., Aleinov, I., Bauer, M., Bauer, S. E., Bhat, M. K., Bleck, R., Canuto, V., Chen, Y. H., Cheng, Y., Clune, T. L., Del Genio, A., de Fainchtein, R., Faluvegi, G., Hansen, J. E., Healy, R. J., Kiang, N. Y., Koch, D., Lacis, A. A., LeGrande, A. N.,

Lerner, J., Lo, K. K., Matthews, E. E., Menon, S., Miller, R. L., Oinas, V., Oloso, A. O., Perlwitz, J. P., Puma, M. J., Putman, W. M., Rind, D., Romanou, A., Sato, M., Shindell, D. T., Sun, S., Syed, R. A., Tausnev, N., Tsigaridis, K., Unger, N., Voulgarakis, A., Yao, M. S., & Zhang, J. (2014). Configuration and assessment of the GISS ModelE2 contributions to the CMIP5 archive. *Journal of Advances in Modeling Earth Systems, 6*(1), 141-184. doi:doi:10.1002/2013MS000265

Schwarz, J. P., Spackman, J. R., Gao, R. S., Watts, L. A., Stier, P., Schulz, M., Davis, S. M., Wofsy, S. C., and Fahey, D. W. (2010), Global-scale black carbon profiles observed in the remote atmosphere and compared to models, Geophys. Res. Lett., 37, L18812, doi:10.1029/2010GL044372.

Sherwood, S. C., Bony, S., Boucher, O., Bretherton, C., Forster, P. M., Gregory, J. M., & Stevens, B. (2015). Adjustments in the Forcing-Feedback Framework for Understanding Climate Change. *Bulletin of the American Meteorological Society, 96*(2), 217-228. doi:10.1175/bams-d-13-00167.1

Smith, C. J., Kramer, R. J., Myhre, G., Forster, P. M., Soden, B. J., Andrews, T., Boucher, O., Faluvegi, G., Fläschner, D., Hodnebrog, Ø., Kasoar, M., Kharin, V., Kirkevåg, A., Lamarque, J.-F., Mülmenstädt, J., Olivié, D., Richardson, T., Samset, B. H., Shindell, D., Stier, P., Takemura, T., Voulgarakis, A., & Watson-Parris, D. (2018). Understanding Rapid Adjustments to Diverse Forcing Agents. *Geophysical Research Letters, 45*(21), 12,023-012,031. doi:10.1029/2018GL079826

Stjern, C. W., Samset, B. H., Myhre, G., Forster, P. M., Hodnebrog, Ø., Andrews, T., Boucher, O., Faluvegi, G., Iversen, T., Kasoar, M., Kharin, V., Kirkevåg, A., Lamarque, J.-F., Olivié, D., Richardson, T., Shawki, D., Shindell, D., Smith, C. J., Takemura, T., & Voulgarakis, A. (2017). Rapid Adjustments Cause Weak Surface Temperature Response to Increased Black Carbon Concentrations. *Journal of Geophysical Research: Atmospheres, 122*(21), 11,462-411,481. doi:doi:10.1002/2017JD027326

Zarzycki, C. M., & Bond, T. C. (2010). How much can the vertical distribution of black carbon affect its global direct radiative forcing? *Geophysical Research Letters, 37*(20). doi:10.1029/2010gl044555

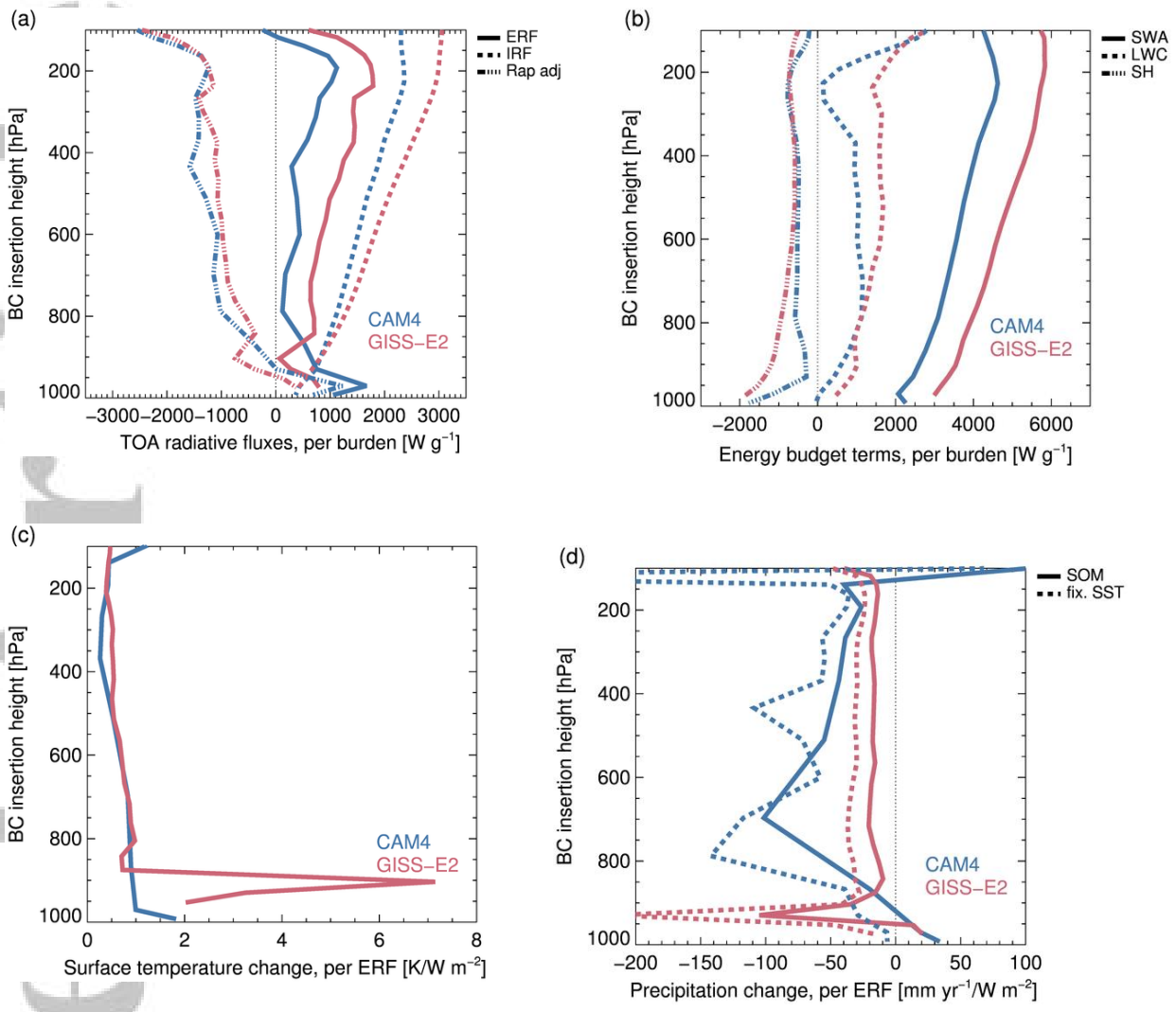

Figure 1: a); Changes in the TOA radiative fluxes per burden for each layer of inserted BC in the fSST runs. The y-axis marks the layer BC was inserted (in hPa). ERF is the net TOA flux (solid), IRF is the TOA direct radiative effect (dotted curve) and Rap adj is the rapid adjustment as the flux at TOA (striped-dotted). b); SW absorption, (solid) LW cooling (dotted) and sensible heat flux (dotted-striped) for each BC layer in the fSST runs, c) Surface temperature response per forcing for each BC layer in the SOM ocean runs (K/Wm^{-2}). and d) Precipitation change per forcing (mm yr^{-1}/W m^{-2}) for each BC layer in the fSST runs and the SOM runs, respectively.

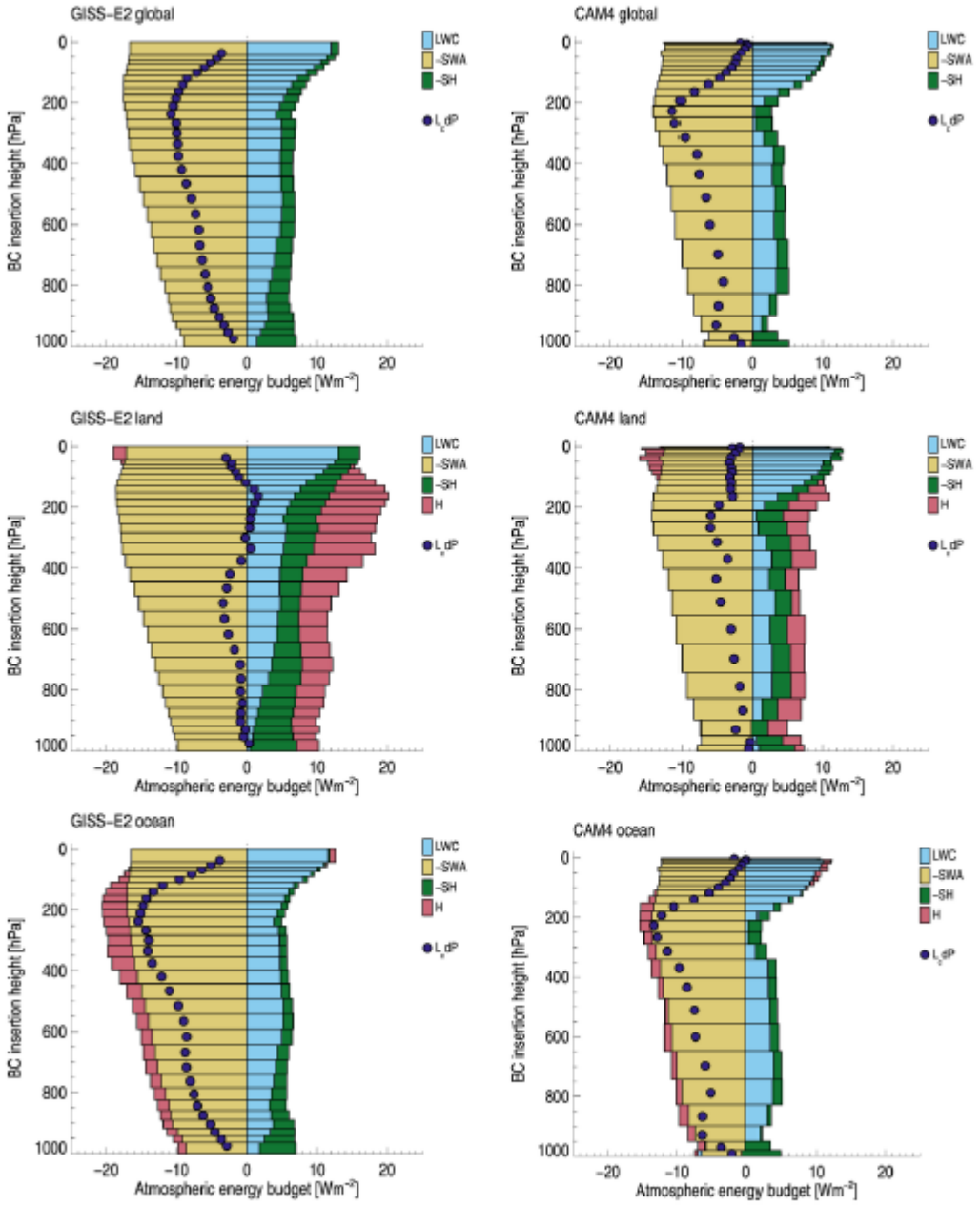

Figure 2: The atmospheric energy budget for each BC insertion for the fast-feedbacks (fSST runs) global average (top), land average (middle) and ocean average (bottom). Each bar represents one simulation (perturbation – baseline). The y-axis marks the altitude of the layer at which BC was inserted. LWC is the longwave cooling, SWA is the shortwave absorption, SH is the sensible heat flux, L_c is the latent heat of condensation, P is precipitation, H is the dry static energy divergence. Note the sign convention, chosen so that positive changes imply a precipitation increase.

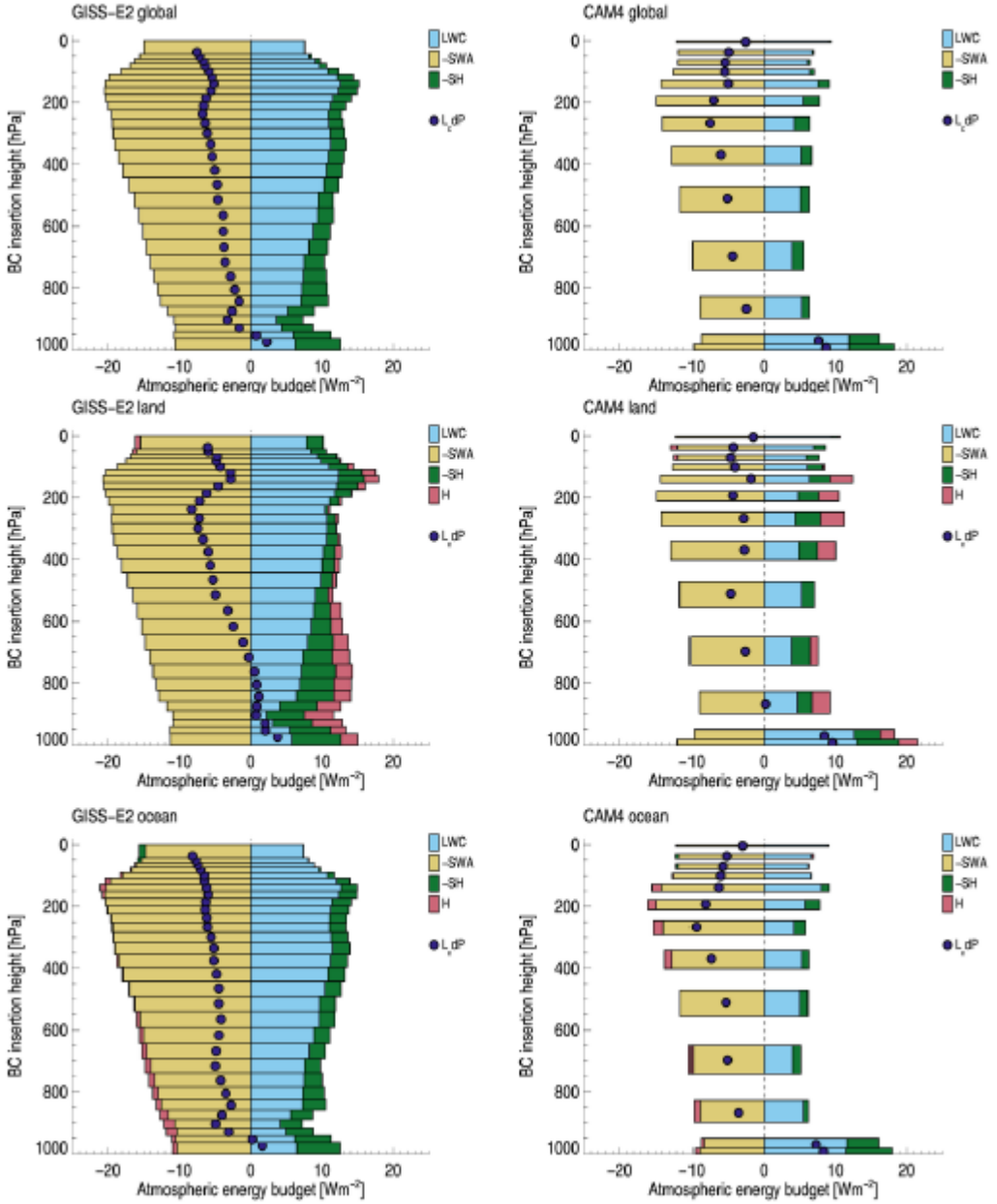

Figure 3: As in Figure 2 , but for the total (fast+slow) response (SOM runs). Note that not all layers were perturbed for CAM4.

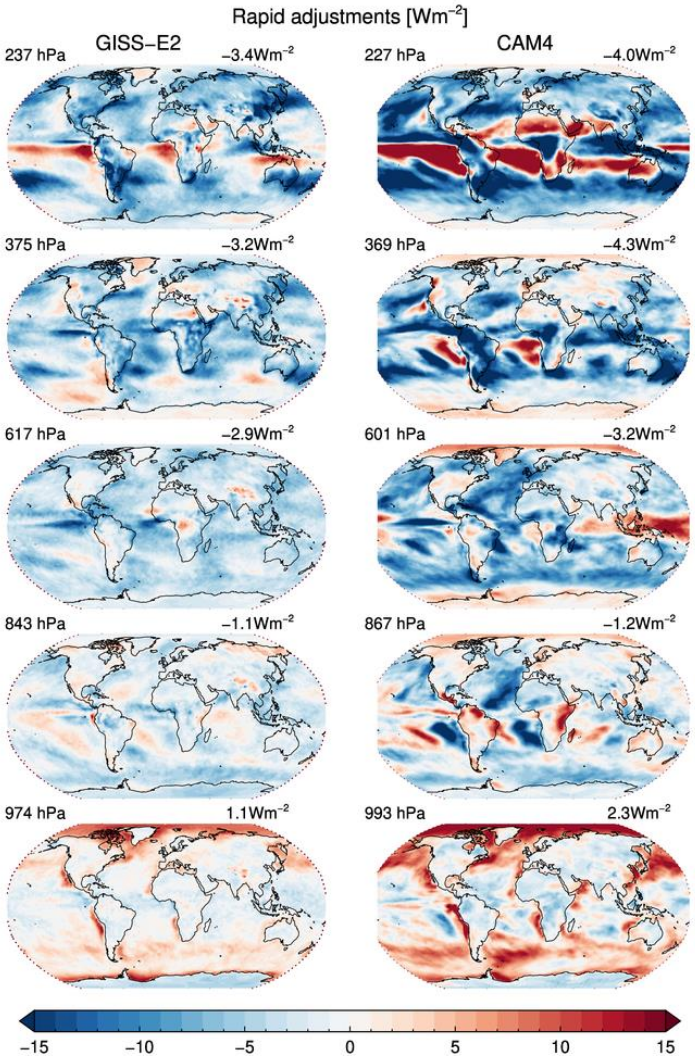

Figure 4: Annual mean change in the rapid adjustments between 5 perturbed fSST runs and the baseline run (fast response). The BC injection height/layer for the perturbed run is specified in hPa, for GISS-E2 (left) and CAM4 (right). Global mean change in rapid adjustments at TOA is given on top of each plot.

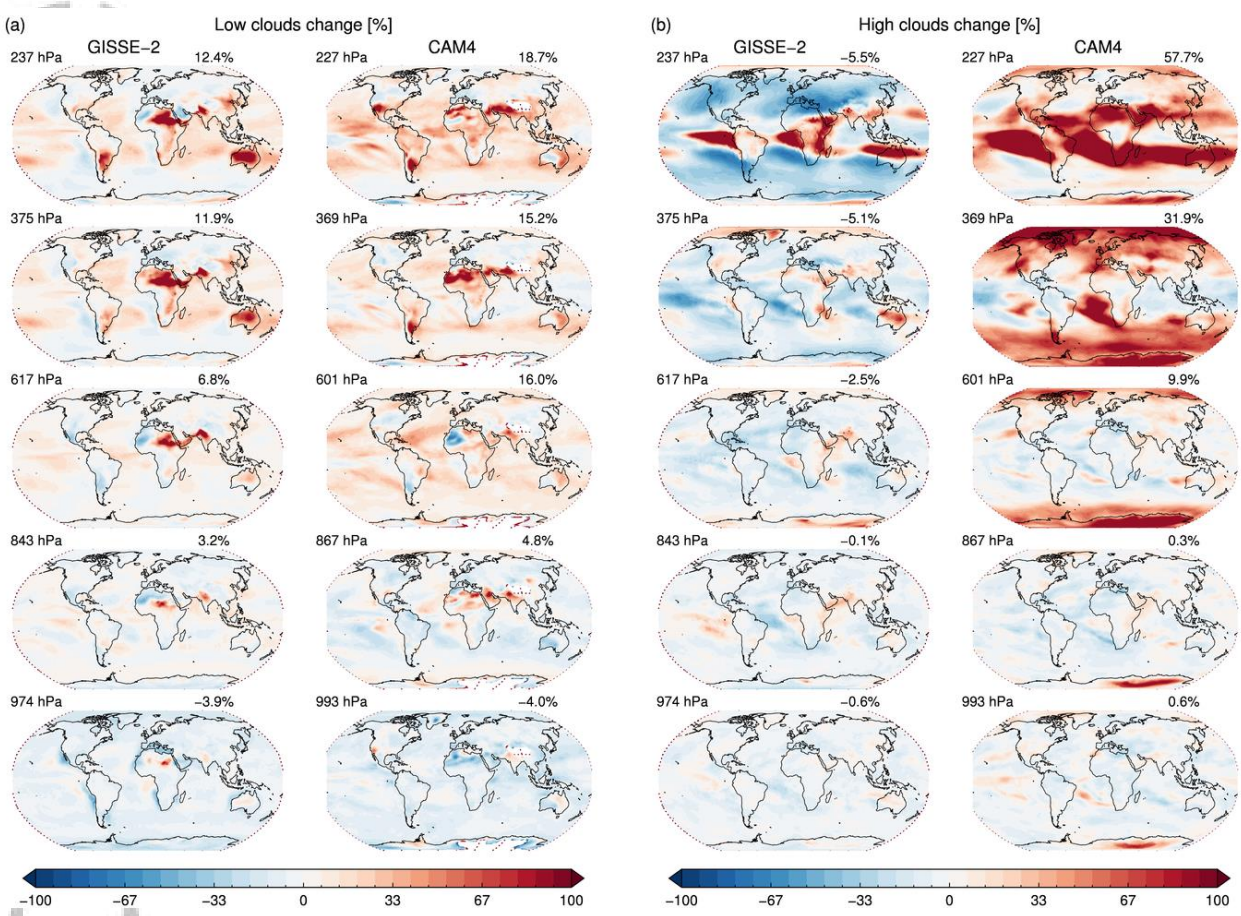

Figure 5: Annual mean relative change [%] in a) low cloud fraction and b) high cloud fraction between 5 perturbed fSST runs and the baseline run (fast response). The model layer with the added BC is specified in hPa, for GISS-E2 (left column) and CAM4 (right column).

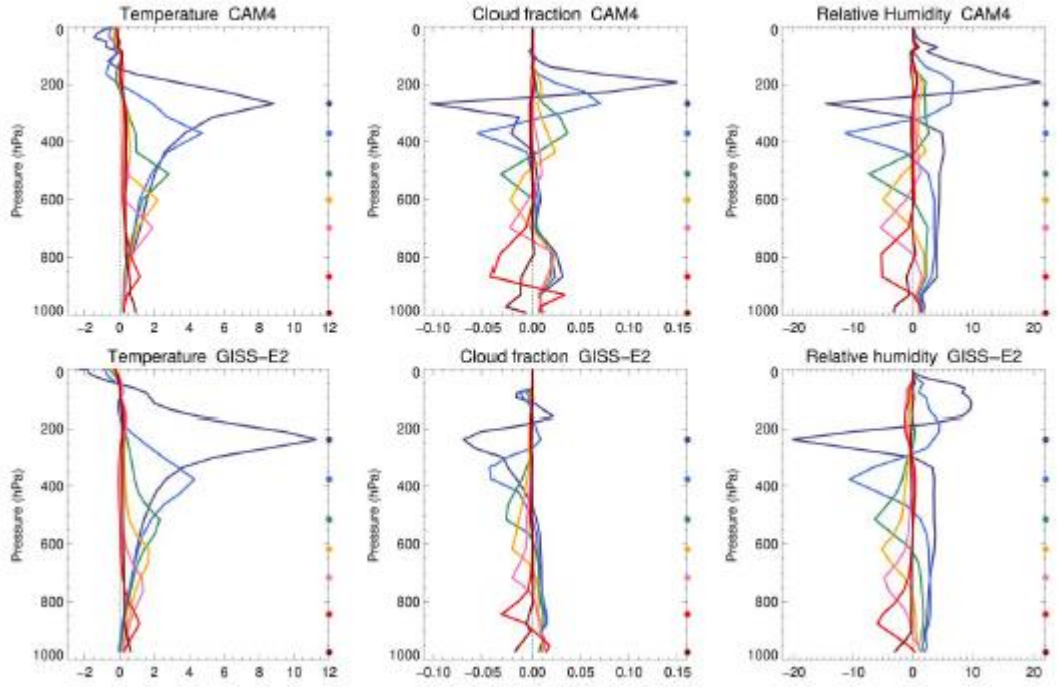

Figure 6: Changes in global mean temperature, relative humidity, and cloud fraction per height at 7 selected perturbed fSST runs and the baseline run, in CAM4 (top) and GISS-E2 (bottom). The dots on the second y-axis represent the BC injection height for each experiment.

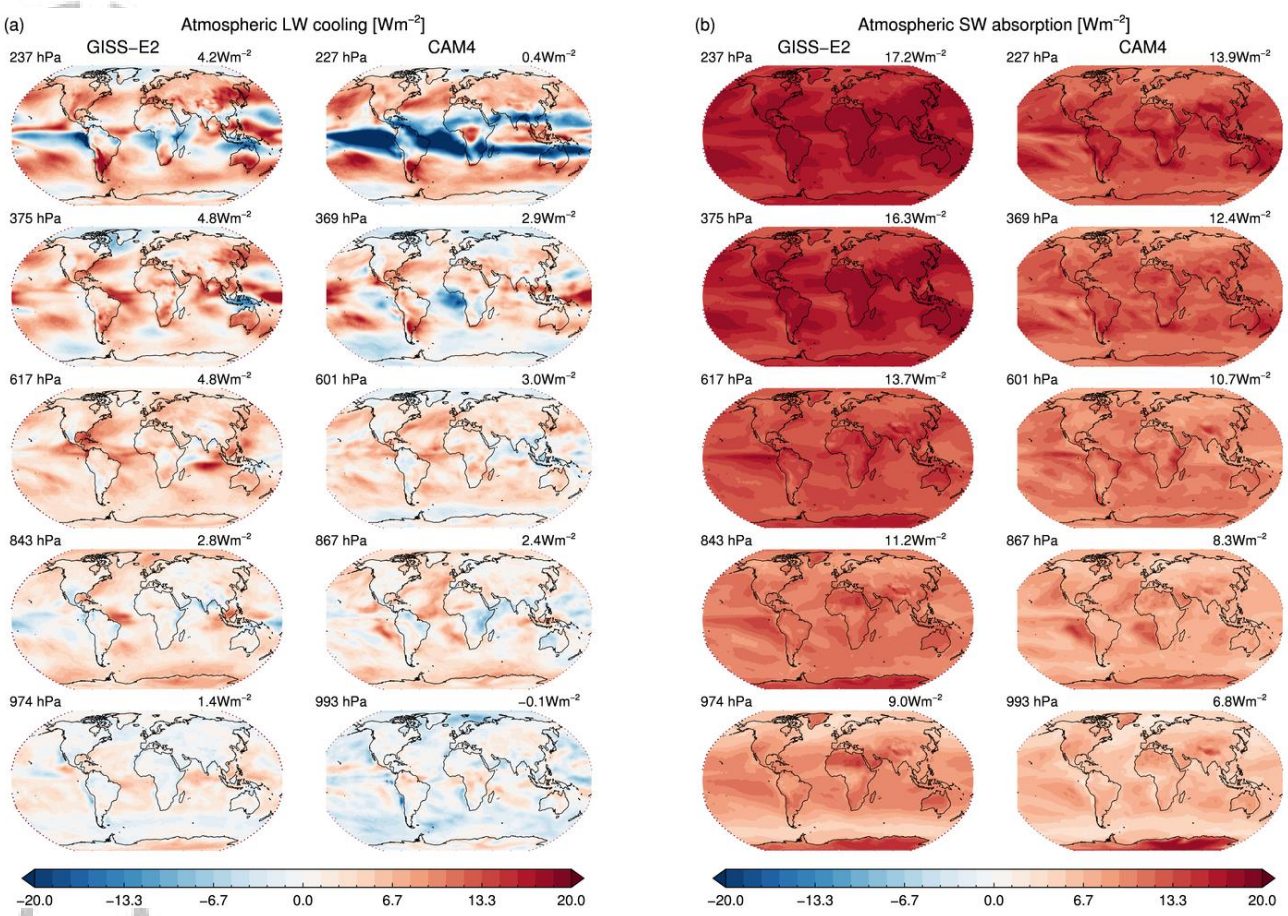

Figure 7: Annual mean change in a) LW cooling and b) SW absorption between 5 perturbed fSST runs and the baseline run (fast response). The BC injection height/layer for the perturbed run is specified in hPa, for GISS-E2 (left) and CAM4 (right).

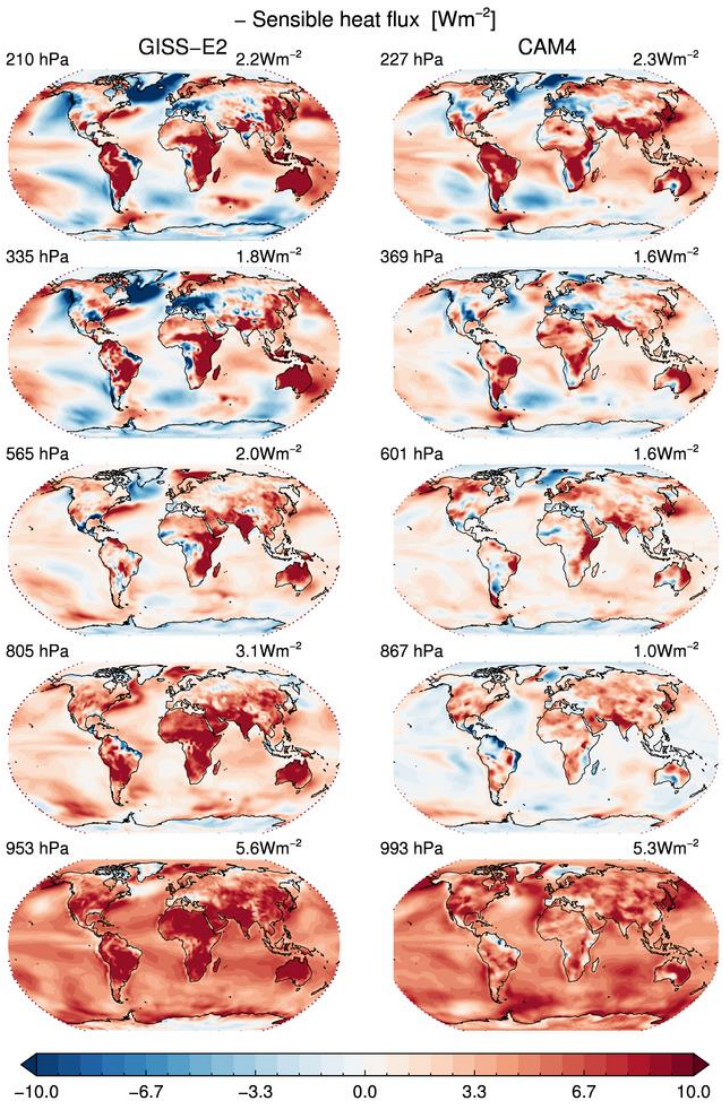

Figure 8: Annual mean change in surface sensible heat between 5 perturbed fSST runs and the baseline run. The BC injection height/layer for the perturbed run is specified in hPa, for GISS-E2 (left) and CAM4 (right).

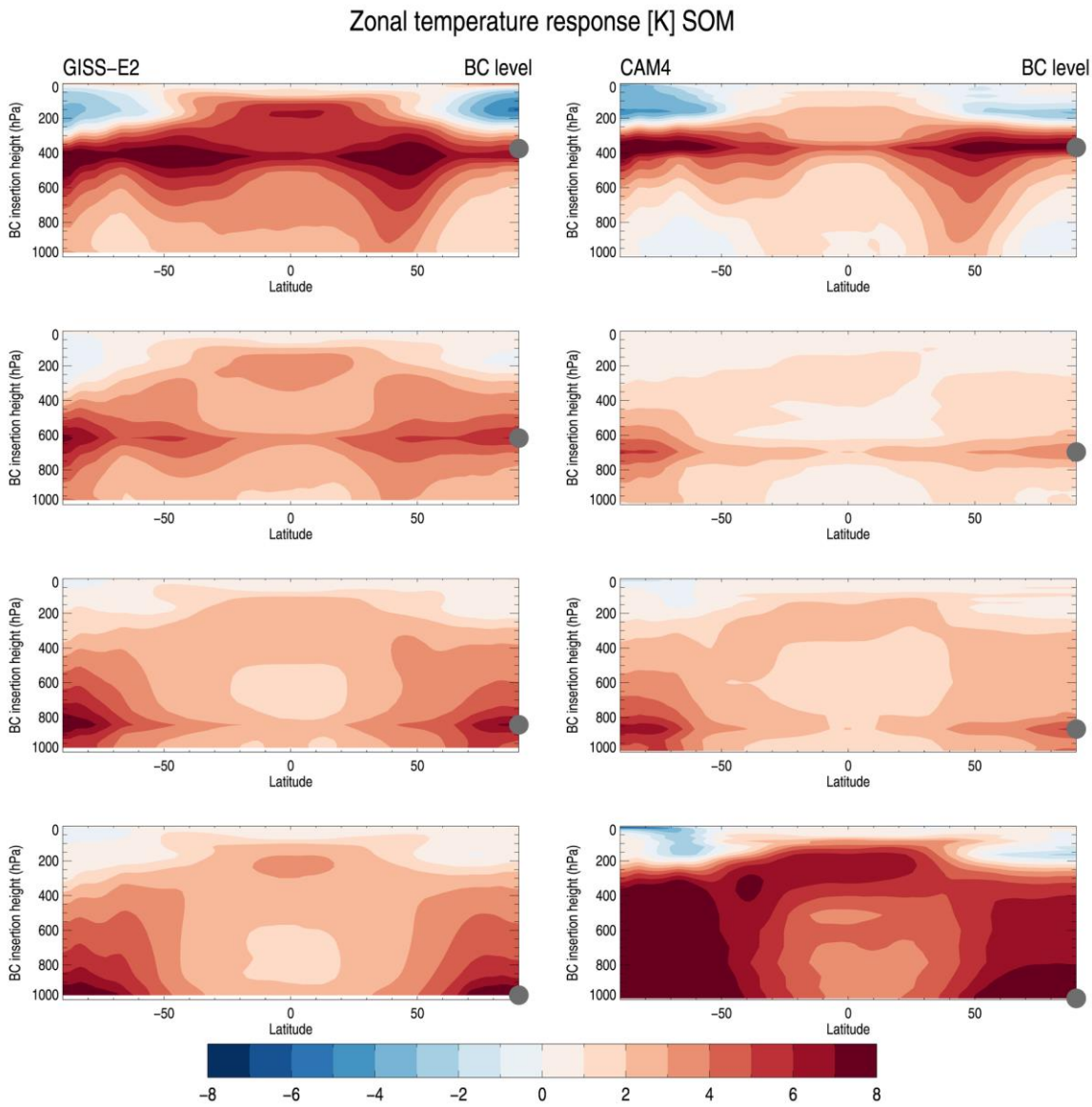

Figure 9: Zonal mean temperature change between four SOM runs and the baseline run for GISS-E2 (left column) and CAM4 (right column), e.g. the total response (fast+slow). The grey dots indicate the BC insertion height.